UV-visible light induced photocatalytic activity of TiO_2 / graphene oxide nanocomposite coatings

A. Datcu,[a,b*] M. L. Mendoza,[b] A. Pérez del Pino,[c] C. Logofatu,[d] C. Luculescu,[a] E. György[a,c*]

[a]National Institute for Lasers, Plasma and Radiation Physics, P. O. Box MG 36, 77125 Bucharest, Romania

[b]Laboratory of Analytical Chemistry, Facultad de Ciencias Naturales y Matemáticas, Escuela Superior Politécnica del Litoral (ESPOL), Campus Gustavo Galindo, km 30-5 Vía Perimetral, Guayaquil, Ecuador.

[c]Instituto de Ciencia de Materiales de Barcelona, Consejo Superior de Investigaciones Científicas, ICMAB-CSIC, Campus UAB, 08193 Bellaterra, Spain.

[d]National Institute for Materials Physics, P. O. Box MG 7, 77125 Bucharest, Romania

Abstract

Titanium dioxide (TiO_2) and TiO_2 - graphene oxide (GO) composite layers were deposited by spin coating technique onto SiO_2 quartz substrates. TiO_2 NPs and GO platelets were used as base materials for the preparation of the starting water/acetone dispersions. Polystyrene (PS) buffer layers were deposited by drop-cast method onto the substrates surface to ensure the adherence of the pure TiO_2/PS and TiO_2-GO/PS composite layer. The surface morphology and physico-chemical properties of the layers have been determined and correlated with their photocatalytic properties. It was found that GO oxygen functional groups are reduced by the presence of TiO_2 NPs in the composite materials. Photodegradation activity under UV–visible light irradiation was studied by measuring the concentration changes in time of organic methylene blue dye in aqueous solutions as well as the chemical oxygen demand for real wastewater samples. The obtained results revealed that the photocatalytic properties of the spin coated composites are determined by the graphene oxide concentration. The effect of the spontaneous reduction of GO in the presence of TiO_2 NPs on the photocatalytic activity of the TiO_2-GO/PS composites is discussed in detail.

Keywords: titanium dioxide/reduced graphene oxide composites; spin-coating; photocatalysis; wastewater; organic pollutant degradation

**Corresponding authors:*

E-mail: datcu.angela@inflpr.ro, Tel.: +40214574550; egyorgy@icmab.es, Tel. +34935801853

1. Introduction

Today's global society is severely affected by environmental pollution, especially water contamination, being water one of the most important and scarcest resources. Consequently, efficient methods have to be developed to eliminate water pollutants, generated by different human activities. In the last decade solar light driven photocatalytic degradation of pollutants has been intensively studied [1, 2]. Semiconductor oxide or sulphide photocatalysts, TiO_2, ZnO, Fe_2O_3, CdS, or ZnS have demonstrated effectiveness for the degradation into less toxic organic compounds of a wide range of organic pollutants [3-8] promoting oxidation and reduction reactions [9]. Among them, TiO_2 is the most investigated oxide semiconductor material, of interest also for other industrial applications such as solar energy conversion [10-12], medical devices and food preparation equipment disinfection [13-15], as well as photocatalytic water splitting [16-18].

However, TiO_2 has two main drawbacks which limit its photocatalytic activity under solar radiation. The large band gap of TiO_2 reduces the absorption range to the UV light, which represents only about 4% of the solar spectrum. The fast recombination rate of the photogenerated charge carriers also reduces the photocatalytic efficiency of TiO_2 [19]. Various methods have been investigated for the development of TiO_2 photocatalyst active both in the UV as well as visible range, representing about 42% of the solar spectrum, and decrease of the charge carriers' recombination rate. These methods include band gap reduction through the creation of oxygen vacancies, addition of cations or anions by chemical doping, as well as coupling with other semiconductors or carbon based nanomaterials [20]. Addition of carbon nanomaterials, activated carbon, fullerenes, carbon nanotubes and graphene was found to offer unique advantages, as chemical inertness and tunable optical and electrical properties [21]. Among them, graphene and reduced graphene oxide (rGO) platelets due to their large specific surface area and high mobility of charge carriers can act as support for transition metal oxide nanoparticles [22-24].

In this work we study the photoactive properties of TiO_2-rGO / polystyrene (PS) composite layers deposited by spin coating technique. The advantages of this method are the low cost, reduced processing time, and the feasibility of thin films fabrication for large-area devices. The photoactive properties of the spin coated composite layers were investigated by the decomposition of both model organic methylene blue (MB) dye solutions and real wastewater samples, under combined UV-visible light irradiation conditions. To date only few works have been reported decomposition of organic pollutants in real sewage water by photocatalysis [25]. Our results demonstrate that the photodegradation efficiency of the TiO_2-rGO/PS composite was significantly higher as compared to

the pure TiO_2 reference layers. A threshold value was determined for the rGO platelets concentration for which the TiO_2-rGO/PS composite films displayed the highest degradation efficiency both in case of model dye as well as organic materials in real wastewater.

2. Experimental

Anatase phase TiO_2 NPs with an average diameter of around 20 nm (Aldrich, 99.5%), graphene oxide (GO) sheets with about 1 μm^2 surface area (NanoInnova Technologies, Madrid, Spain), and PS (Aldrich, average M_w ~192,000) were used as base materials for the preparation of the composite thin films through spin coating technique. The photocatalytic activity of rutile phase TiO_2 mixed with GO platelets was systematically investigated. Methylene blue (MB) ($C_{16}H_{18}ClN_3S$, Fisher Scientific, 93%) was used as model pollutant for the photodegradation process. SiO_2 quartz plates with 1 x 1 cm^2 surface area, cleaned in Piranha solution (H_2O_2:H_2SO_4, 1:3 (v/v)) to render a clean surface, rich in hydroxyl groups, were used as substrates. Subsequently the substrates were washed in ultrasonic bath with distilled water, ethanol, and acetone. For the chemical oxygen demand (COD) dichromate method H_2SO_4 (Baker ACS 97.7%), $K_2Cr_2O_7$ (AR LobaChemie 99.9%), Ag_2SO_4 (Fisher Chemical CS 99.4%), $HgSO_4$ (LobaChemie ACS 98%), $(NH_4)_2Fe(SO_4)_2 \cdot 6H_2O$ (Fisher Chemical ACS 99.99%), and $C_{12}H_8N_2 \cdot H_2O$ (Fisher Scientific) were used as chemical reagents.

30 µL of polystyrene (PS) solution in acetone (1 wt. %) were drop-casted on the surface of the SiO_2 quartz substrates. The obtained PS layers were dried at room temperature. The role of the PS buffer layer is to ensure a better adherence of the TiO_2 and TiO_2-GO coatings to the SiO_2 quartz substrates. The TiO_2/PS and TiO_2-GO/PS composite films were prepared by spin coating method using dispersions of 5 wt.% TiO_2 NPs or mixed dispersions containing 5 wt.% TiO_2 NPs and 1, 2, 3, or 4 wt.% GO platelets in 0.2 g acetone and 0.3 g distilled water. 50 µL of precursor dispersion was dropped onto the previously prepared PS drop-casting layer. This assembly was subjected to spinning operation (600 rpm/s). Subsequently, the substrates coated with TiO_2 or TiO_2-GO/PS films were heat-treated at 65 °C for 5 min on a heating plate in air at atmospheric pressure. The final samples consisted on three identical superposed TiO_2 or TiO_2-GO layers repeating the previously described process.

The surface morphology of the deposited films was investigated by scanning electron microscopy (SEM) with a Carl Zeiss EVO 50 XVP instrument, operated at 30 kV and 10 nA. Raman spectra were registered with the aid of a micro-Raman spectrometer (NRS-7200, JASCO, Japan) using a 532 nm solid-state laser as an excitation source. The laser light was focused on the sample surface by means

of a short working distance 100× objective lens with a numerical aperture (NA) = 0.9 (Olympus, Tokyo, Japan) to a spot of about 2 μm diameter. The nominal power of the laser was set at 5 mW. The spectral resolution was 4 cm^{-1}. Each spectrum was acquired in 60 s and 10 scans. To obtain information about the chemical bonds between the elements, X-ray photoelectron spectroscopy (XPS) studies were performed with the aid of a SPECS XPS spectrometer (SPECS Surface Nano Analysis GmbH), based on Phoibos 150 electron energy analyzer operated in constant energy mode. A monochromatic X-ray source (Al Kα line, 1486.74eV) was used for excitation. The measurements were made in an ultrahigh vacuum at a 10^{-7} Pa residual pressure. The high resolution spectra were acquired over small ranges of binding energy (20 eV) with a minimum 20 scans using a 0.05 eV step and 10 eV pass energy. The obtained data were analyzed using SI_SDPv7.0 software.

The adsorption and photocatalytic activity of the TiO_2/PS and TiO_2-GO/PS films was studied by measuring the time evolution of organic MB dye concentration in aqueous solution and COD reduction of the organic waste degradation, in dark conditions as well as under simultaneous UV-visible light irradiation. The photocatalytic efficiency of the thin films was tested also for real wastewater degradation. The photodegradation reactor consists of an aluminium cylindrical container. One 18 W Philips lamp emitting in the UV range 340–400 nm, with maximum emission wavelength of 365 nm providing and intensity of around 1 mW/cm^2, and two 18 W Philips visible, 400 – 700 nm light lamps, with maximum emission wavelength of 558 nm and around 0.5 mW/cm^2 intensity were used for photodegradation experiments. The samples were immersed in 10 mL MB solutions with 1.25 x 10^{-5} M initial dye concentration (C_0). All these components were placed in an aluminum housing to prevent interfering of external light in the photodegradation experiments. During the photodegradation experiments, the absorbance of the solution was measured at 665 nm wavelength, which corresponds to the peak absorbance of MB in the UV–visible spectral range, with the aid of a Thermo Scientific spectrophotometer UV Visible SPECTRONIC 200E. Based on the MB dye concentration–absorbance calibration curve, the adsorption and photocatalytic efficiency (η) of the samples was calculated using the formula $\eta = (C_0\text{-}C) \times 100/C_0$, where C is the MB concentration in the aqueous solution measured at regular time intervals.

The degradation of the organic materials in real wastewater samples was evaluated through COD reduction under simultaneous UV–visible light irradiation during 3 h, using the same photoreactor as for the degradation of model MB dye solutions. The conventional dichromate method was used to determine the COD values (Standard Methods for the Examination of Water and Wastewater, APHA, AWWA, WEF). The spin–coated samples were immersed in untreated domestic wastewater with slightly brown and turbid appearance coming from a semi-urban area (Marcelino Maridueña,

Ecuador, a city with about 11000 inhabitants). 20 mL diluted sewage (10 mL distilled water and 10 mL wastewater) was used, with initial COD_0 value of 160 mg/L. The contaminants reduction efficiency was calculated using the formula $\eta = (COD_0 - COD_{3h}) \times 100/COD_0$ where COD_{3h} is the final COD value after 3 h of UV-visible irradiation. Reference measumerents in the absence of catalysts (blank) or in the absence of illumination (dark adsorption test) were also carried out.

3. Results and discussion

Fig. 1 shows the SEM images of TiO_2/PS film prepared from a dispersion containing TiO_2 NPs (Fig. 1a) and composite TiO_2-GO/PS films containing 2 and 4 wt. % GO (Fig. 1b-d). As can be observed in Fig. 1a the initial TiO_2 NPs are forming large, hundreds of nm sized clusters on the substrate surface, giving a sponge-like morphology. The TiO_2 NPs covered almost entirely the GO platelets in case of the TiO_2-GO/PS films. However, surface areas with uncovered GO platelets can be also detected (Fig. 1c, d).

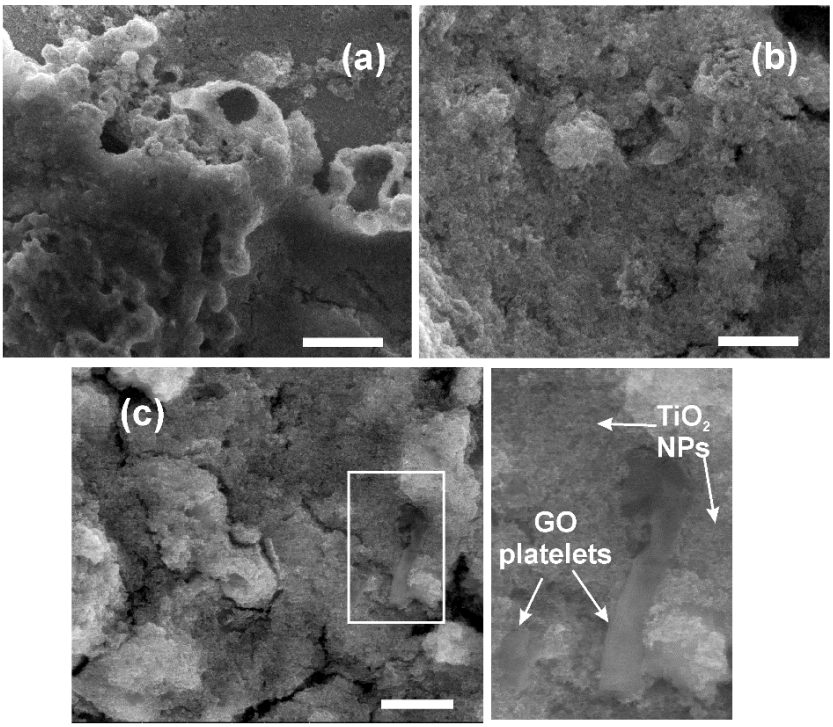

Fig.1. SEM images of TiO_2/PS and TiO_2-GO/PS films obtained by spin coating method from dispersions containing (a) 5 wt. % TiO_2 NPs, as well as 5 wt. % TiO_2 NPs and (b) 2 and (c) 4 wt.% GO platelets; (d) high magnification SEM image of the marked area in Fig. 1c. Scale bars correspond to 5 μm in all images.

Fig. 2 shows the micro-Raman spectrum of the TiO_2-GO/PS nanocomposite thin film obtained from the dispersion containing 5 wt.% TiO_2 anatase phase NPs and 4 wt. % GO platelets. The anatase structure belongs to the tetragonal space group of *I*41/*amd* with six allowed Raman transitions, one A_{1g}, two B_{1g}, and three E_g modes, A_{1g} overlapping with the B_{1g} mode in the 510 – 520 cm^{-1} wavenumber range [26]. In the spectrum of the TiO_2-GO nanocomposite thin film the lines situated at 394, 513, and 632 cm^{-1} can be assigned to the $B_{1g(1)}$, $A_{1g} + B_{1g(2)}$, and $E_{g(3)}$ Raman-active modes of the anatase phase TiO_2 [27-29]. The broad lines at around 1353 and 1598 cm^{-1} belong to the D and G vibrational modes of carbon materials [30-32]. The G band corresponds to the first-order scattering of E_{2g} phonons from sp^2-bonded carbon atoms of the graphite lattice, while the D band is attributed to structural imperfections in graphene and vibrations of sp^3-hybridized carbon atoms of C–O bonds [31, 32].

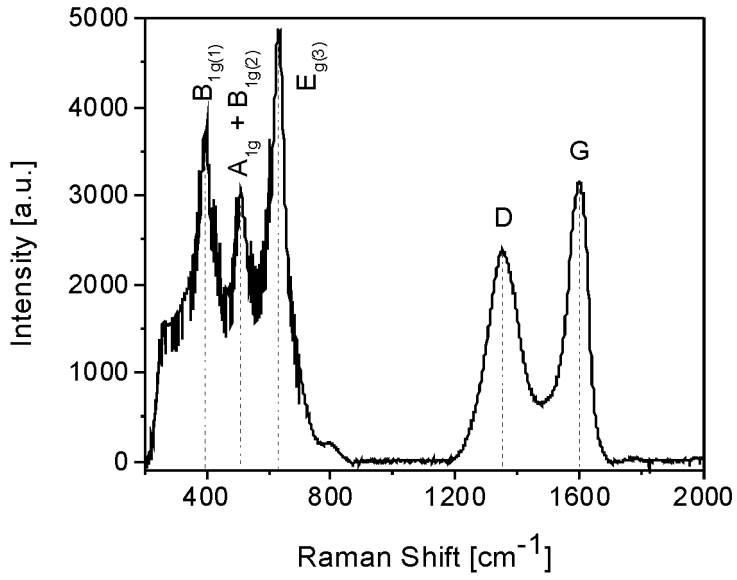

Fig. 2. Micro-Raman spectrum of TiO_2-GO/PS film obtained from the 5 wt. % TiO_2 NPs and 4 wt. % GO platelets dispersion

To further examine the chemical bonding states on the surface of the TiO_2-GO/PS composite samples, XPS investigations were performed. The C 1s spectra of GO drop-cast reference sample (a) as well as of the TiO_2-GO/PS composite films obtained from the 5 wt. % TiO_2 NPs and 2 (b) and 4 wt. % GO platelets (c) dispersions are shown in Fig. 3. The spectrum of the GO drop-cast sample was deconvoluted in three lines. The line situated at 284.8 eV binding energy is attributed to graphite-like sp^2 C, C=C bonds of the conjugated honeycomb lattice while the lines situated at higher 286.6 and 288.1 eV binding energies can be assigned to C-O single bonds in C–O–C epoxy C–OH hydroxyl groups, as well as C=O double bonds in C=O carbonyl and HO–C=O carboxyl groups of graphene oxide, respectively [33 - 35]. The lines' position in the C1s spectra of the TiO_2-GO/PS coatings (Fig.

3 b,c) is very similar to that of the reference GO sample. However, the intensity of the lines corresponding to the oxygen containing functional groups of GO is much reduced in case of the TiO_2-GO/PS coatings as compared to the reference drop-cast GO sample (Fig. 3a), indicating a diminishment of the number of oxygen containing functional groups in the presence of TiO_2 NPs. Reduction of graphene oxide was obtained by several methods such as high temperature treatment under ultra-high vacuum [33, 36], or chemical treatment with different reducing agents as sodium borohydride, benzylamin, or hydrazine [37 - 41], treatment with green reductants such as L-ascorbic acid (L-AA), D-glucose (D-GLC) and tea polyphenol (TP) [42], or laser techniques [43 - 44]. The photocatalytic reduction of oxygen functional group of GO has been obtained by mixing GO with TiO_2 in ethylene glycol using a xenon arc lamp [45] and more recently the spontaneous reduction of GO was also reported in case of TiO_2-GO drop casted composite samples, under normal atmospheric conditions [46].

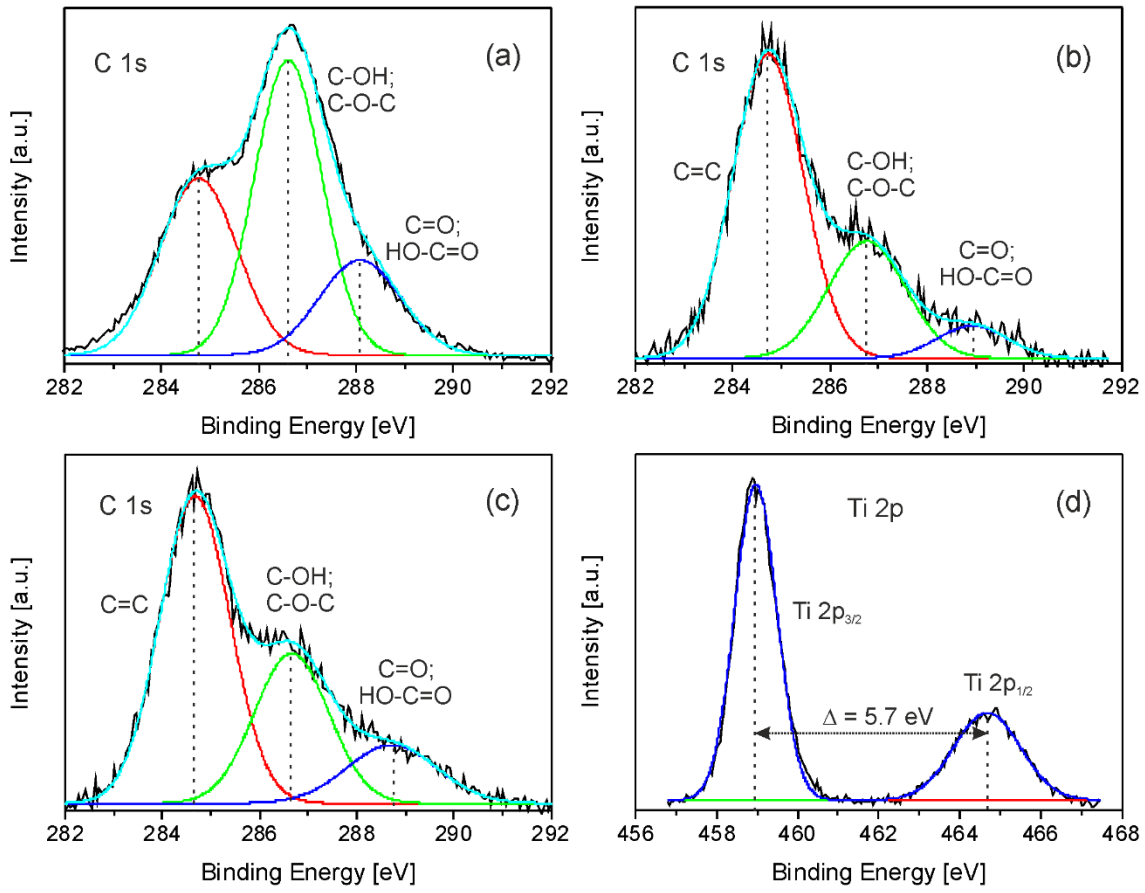

Fig. 3. C 1s XPS spectra of (a) GO drop-cast reference sample as well as TiO_2-GO/PS composite films obtained from the 5 wt. % TiO_2 NPs and (b) 2 and (c) 4 wt. % GO platelets dispersions; (d) Ti 2p XPS spectrum of TiO_2-GO/PS composite film obtained from the 5 wt. % TiO_2 NPs and 4 wt. % GO platelets dispersion.

With the purpose to quantify the level of GO reduction we calculated the oxide peaks area and the total C1s peak area ratios for the reference GO as well as the composite TiO_2-GO/PS thin films. A I_{C-O}/I_C peak ratio of around 0.48 was calculated for the reference GO sample. The ratio decreases to around 0.27 in case of the sample obtained from the 5 wt.% and 2 wt. % GO dispersion. However, a slight higher value, around 0.30 was calculated for the sample with higher, 4 wt. % GO platelets concentration. A similar trend was observed for the C=O double bonds. The reference sample has a $I_{C=O}/I_C$ peak ratio of about 0.18. This value decreases to around 0.06 for the TiO_2-GO/PS composite sample ontaining 2 wt. % GO, but increases to around 0.14 in case of the sample with higher, 4 wt. % GO platelets concentration.

The Ti2p XPS spectrum of the composite TiO_2-GO/PS thin film containing 4 wt. % GO platelets is presented in Fig. 3d. The spectrum is a doublet, composed by two peaks, $Ti2p_{3/2}$ and $Ti2p_{1/2}$ centered at 458.9 and 464.6 eV binding energy values, respectively. The binding energy values and the spin–orbit splitting equal to 5.7 eV as well as the symmetrical shape of the peaks indicate a chemical state of Ti^{4+} of stoichiometric TiO_2 [47-50]. The Ti2p spectra of the TiO_2 as well as composite TiO_2-GO/PS thin film are identical, irrespective of the GO platelets concentration.

The dark adsorption and photodegradation efficiency of the samples were systematically investigated using MB model dye solutions (Fig. 4I, II) as well as real wastewater (Fig. 5). In order to establish the average deviation, we used series of samples consisting of twin samples. A mean average deviation of around 0.4 % was calculated. The adsorption and photocatalytic efficiency after 7 h storage in dark or UV-visible light exposure time are presented in Table I. The last column in Table I contains the photocatalytic efficiencies of the samples, subtracting the dark adsorption.

The MB adsorption capacity of the pure TiO_2 sample was found to be very low, around 5.6 %, the adsorption equilibrium being reached after around 60 min. storage time. On the other hand, the adsorption efficiency of the composite TiO_2-GO thin film was found to be significantly higher, reaching around 26.2 % after a storage time of 7 h for the sample with the highest, 4 wt. % GO platelets concentration (Fig. 4I). The significant adsorption capacity of the TiO_2-GO thin film is due to the presence of the GO platelets. The high adsorption of organic pollutants in aqueous solutions was attributed to electrostatic interactions between the GO surface and dye molecules, due to the cationic nature of the dye molecules and π–π interactions between the phenyl rings of dye molecules and the GO surface [52, 53]. Besides electrostatic and π–π interactions, hydrogen-bonding interactions between the carboxyl groups of GO and MB dye molecules can also take place [54].

Table I. Dark adsorption and photocatalytic efficiency after 7 h storage in dark or UV-visible light exposure time

Samples	Dark adsorption efficiency [%]	Photocatalytic efficiency+ adsorption [%] (1)	Photocatalytic efficiency+ adsorption [%] (2)	Photocatalytic efficiency+ adsorption average [%]	Photocatalytic efficiency [%]
5wt.%TiO_2	5.6	22.4	22.7	22.5	16.9
5wt.%TiO_2+ 1wt.%GO	20.1	28.9	28.6	28.8	8.7
5wt.%TiO_2+ 2wt.%GO	21.4	35.9	36.4	36.1	14.7
5wt.%TiO_2+ 3wt.%GO	21.0	39.7	38.2	39.0	18.0
5wt.%TiO_2+ 4wt.%GO	26.2	29.5	30.5	30.0	3.8

The MB photodegradation efficiency, which includes also the contribution of adsorption, of the pure TiO_2/PS as well as TiO_2-GO/PS composite thin films under UV-visible light irradiation are shown in Fig. 4II. The self-degradation of MB exposed to UV-visible light irradiation in the absence of catalysts remain below 4.5 % of the initial MB concentration in the irradiated solution. The photocatalytic efficiency of the TiO_2-GO/PS composite thin films is higher than that of the pure TiO_2/PS film and increases gradually with the increase of the GO platelets concentration, reaching around 40 % in case of the sample containing 3 wt.% GO platelets. However, the degradation efficiency of the composite films with the highest, 4 wt.% GO platelets concentration is lower, around 30 %. This difference is even higher if the contribution of MB adsorption is subtracted (Table I). As can be observed in Fig. 4I the adsorption efficiency of the samples increases with the increase of the GO platelets concentration.

UV radiation with 365 nm emission maximum corresponds to a photon energy of 3.4 eV, exceeding the band gap of anatase phase TiO_2, 3.2 eV. Thus, UV light irradiation of TiO_2 in aqueous media leads to the generation of electron-hole pairs (1) which contribute to the formation of reactive oxidative species (ROSs), as $O_2^{\cdot -}$ superoxide anions (2) and $HO^{\cdot}$ hydroxyl (3) radicals [55-58]:

$$TiO_2 + h\nu[UV] \rightarrow TiO_2(e^-) + TiO_2(h^+) \quad (1)$$

$$TiO_2(e^-) + O_{2\ ads} \rightarrow O_2^{\cdot -} \quad (2)$$

$$TiO_2(h^+) + H_2O_{ads} \rightarrow TiO_2 + (HO^{\cdot}) + H^+ \quad (3)$$

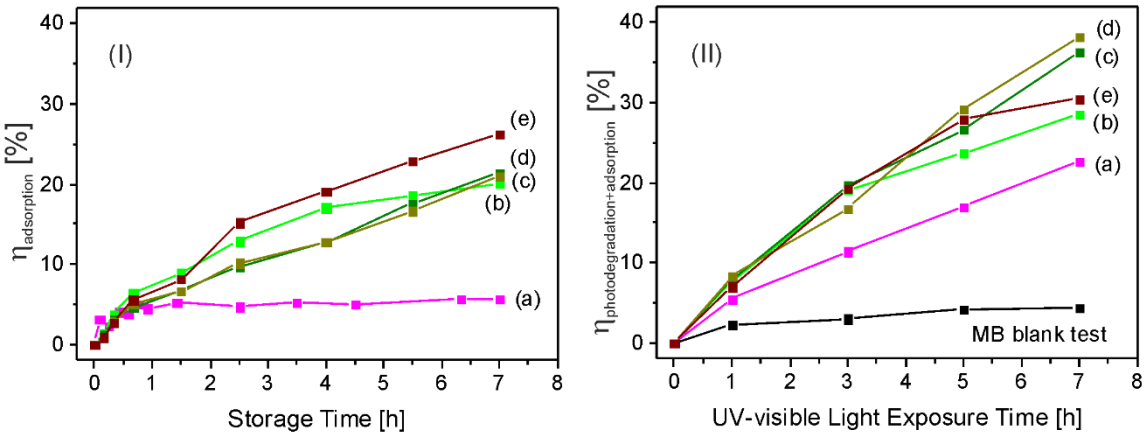

Fig. 4. (I) MB dark adsorption efficiency and (II) MB photocatalytic decomposition and adsorption efficiency under UV-visible light irradiation of (a) pure TiO_2/PS thin film obtained from the 5 wt. % TiO_2 NPs dispersion and TiO_2-GO/PS composite films obtained from the 5 wt. % TiO_2 NPs and (b) 1, (c) 2, (d) 3 and (e) 4 wt. % GO platelets dispersions, measured at regular time intervals.

In case of the TiO_2-rGO/PS composites rGO can also contribute to the generation of electron-hole pairs under UV light irradiation (4) and thus to the formation of ROSs (5, 6) leading to enhanced photocatalytic efficiency:

$$rGO + hv[UV] \rightarrow rGO(e^-) + rGO(h^+) \quad (4)$$

$$rGO(e^-) + O_{2\ ads} \rightarrow O_2^{\cdot -} \quad (5)$$

$$rGO(h^+) + H_2O_{ads} \rightarrow rGO + (HO^{\cdot}) + H^+ \quad (6)$$

Subsequently, organic dye molecules are decomposed by the generated ROSs (6, 7):

$$(HO^{\cdot}) + MB \rightarrow CO_2 + H_2O \quad (6)$$

$$O_2^{\cdot -} + MB \rightarrow CO_2 + H_2O \quad (7)$$

The higher photocatalytic efficiency of TiO_2-GO/PS composite films as compared to pure TiO_2/PS layer can be also attributed to charge separation and charge transfer mechanisms preventing the recombination of photogenerated hole-electron pairs [59, 60]. All described mechanisms, generation of electron-hole pairs by rGO as well as charge separation and charge transfer properties are determined by the optical [61] and electrical properties of GO platelets [62] defined in turn by the amount of oxygen containing functional groups. XPS investigations revealed that GO reduction is less effective in case of the TiO_2-GO/PS sample containing 4 as compared to those inclosing 2 wt. % GO platelets (Fig. 3b,c). These features could explain the lower photocatalytic efficiency of the TiO_2-GO/PS sample with the highest 4 wt.% GO platelets concentration.

Conversely, degradation of organic molecules under visible light irradiation induced by the generation of charge carriers cannot be considered as a possible mechanism due to the large band gaps of TiO_2 and rGO. However, visible light irradiation can be absorbed by the dye molecules acting as sensitisers in the degradation process [63-66]. The generated photoelectrons can be transferred to the conduction band of TiO_2 and could be trapped by the adsorbed O_2 molecules on the photocatalysts surface, further contributing to the generation of ROSs. Thus, under visible light irradiation besides self-degradation, MB molecules are degraded by the generated ROSs through dye-sensitized reactions [63-65].

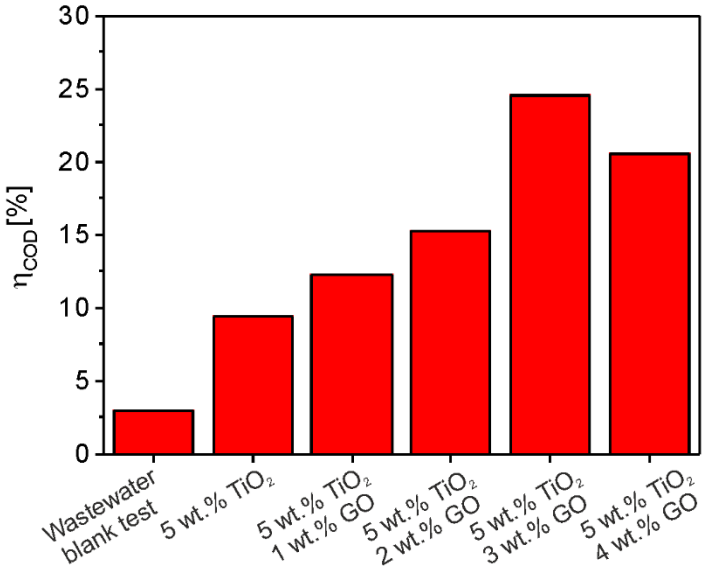

Fig 5. COD efficiency of wastewater after 3 h reaction time in the presence of TiO_2/PS film obtained from the 5 wt.% TiO_2 NPs dispersion and TiO_2-GO/PS composite films obtained from the 5 wt. % TiO_2 NPs and 1, 2, 3, and 4 wt. % GO platelets dispersions under UV-visible light irradiation.

The wastewater contaminants reduction efficiency calculated from the COD values follows the same trend as observed during photodegradation of MB, being the highest for the TiO_2-GO/PS thin film containing 3 wt.% GO platelets (Fig. 5). The degradation efficiency of the composite layer with a GO platelets concentration of 3 wt.% is around 260 % higher as compared to the pure TiO_2/PS layer. The photodegradation experiments were performed under identical experimental conditions as used for the MB degradation tests, substituting the MB solutions with real wastewater samples.

Conclusions

Pure rutile TiO_2/PS and rutile TiO_2-GO/PS coatings were obtained by spin coating deposition technique. The chemical composition of the layers was analyzed by micro-Raman spectroscopy and XPS. The oxygen functional groups of GO were reduced in the presence of TiO_2 NPs. The photocatalytic efficiency of the samples was found to increase gradually with the inclusion of GO platelets in the composites. The TiO_2-GO/PS composite sample with 3 wt. % GO platelets concentration had the highest photocatalytic efficiency under simultaneous UV-visible light irradiation, both in case of MB dye as well as wastewater degradation. The higher photocatalytic efficiency of TiO_2-GO/PS composites as compared to the reference TiO_2/PS layers is attributed to charge separation and charge transfer properties of GO preventing the recombination of photogenerated hole-electron pairs. Moreover, under UV light irradiation GO can also participate in the electron-hole pairs generation process. Dye-sensitized reactions contribute to the degradation process under visible light irradiation. At higher GO concentrations the photocatalytic activity of the composite material decreased the most probably due to less efficient reduction of GO platelets in the presence of the same amount of TiO_2 NPs, influencing both the generation of electron-hole pairs by rGO as well as charge separation and transfer properties.

Acknowledgements

The authors thank the financial support of the “Prometeo Program” of the National Secretary of Education, Science, Technology and Innovation of the Ecuadorian Government (SENESCYT), the Executive Unit for Financing Higher Education, Research, Development and Innovation of the Romanian Ministry of Education and Scientific Research under the contract PN-III-P2-2.1-PED-2016-1043 and Nucleus program at NILPRP under project 4N/9.03.2016 (16 47 01 02).

References

1. A. Alinsafi, F. Evenou, E.M. Abdulkarim, M.N. Pons, O. Zahraa, A. A. Benhammou, Yaacoubi, A. Nejmeddine, Dyes Pigm. 74 (2007) 439-455.
2. M.A. Lazar, S. Varghese, S.S. Nair, Catalysts 2 (2012) 572-601.
3. K.M. Lee, C.W. Lai, K.S. Ngai, J.C. Juan, Water. Res. 88 (2016) 428-448.
4. M. Mishra, D.M. Chun, Appl. Catal. A 498 (2015) 126–141.
5. S. Qian, C. Wang, W. Liu, Y. Zhu, W. Yao, X. Lu J. Mater. Chem. 21(2011) 4945-4952.
6. C.C. Wang, J.R. Li, X.L. Lv, Y.Q. Zhang, G. Guo, Energy Environ. Sci. 7 (2014) 2831–2867.
7. L. Wang, M. Wen, W. Wang, N. Momuinou, Z. Wang, S. Li, J. Alloy Compd. 683 (2016) 318-328.
8. X. Kang, S. Chen, J. Mater. Sci. 45 (2010) 2696–2702.
9. A. Fujishima, T.N. Rao, D.A.Tryk, J. Photochem. Photobiol. C: Photochem. Rev. 1(2000) 1-21.
10. G. Liu, L.C. Yin, J. Wang, P. Niu, C. Zhen, Y. Xie, H.M. Cheng. Energy. Environ. Sci. 5 (2012) 9603–9610.
11. M. Samir, M. Salama, NK. Allam, J. Mater. Chem. A 4 (2016) 9375–9380.
12. J.F. Houlihan, D.P. Madacsi Mat. Res. Bull. 11 (1976) 1191-1198.
13. G. Liu, N. Hoivik, K. Wang, H. Jakobsen, Sol. Energ. Mat. Sol. C 105 (2012) 53–68.
14. L. Visai, L. De Nardo, C. Punta, L. Melone, A. Cigada, M. Imbriani, C.R. Arciola, Int. J. Artif. Organs. 34 (2011) 929-946.
15. J. Gamage, Z. Zhang, Int. J. Photoen. Article ID 764870 (2010).
16. N.G. Chorianopoulos, D.S. Tsoukleris, E.Z. Panagou, P. Falaras, G.J.E. Nychas, Food Microbiol. 28 (2011) 164-170.
17. M. Ni, M.K.H. Leung, D.Y.C. Leung, K. Sumathy, Renew. Sust. Energ. Rev. 11 (2007) 401–425.
18. R. Dholam, N. Patel, M. Adami, A. Miotello, Int. J. Hydrogen Energ. 34 (2009) 5337–5346.
19. J. Schneider, M. Matsuoka, M. Takeuchi, J. Zhang, Y. Horiuchi, M. Anpo, D.W. Bahnemann, Chem. Rev. 114 (2014) 9919−9986.
20. J. Chen, F. Qiu, W. Xu, S. Cao, H. Zhu, Applied Catalysis A: General 495 (2015) 131–140.
21. R. Leary, A. Westwood, Carbon 49 (2011) 741–772.
22. B.A. Bhanvase, T.P. Shende, S.H. Sonawane, Environ. Technol. Rev. 6 (2016) 1–14.
23. X. Li, J. Yu, S. Wageh, A.A. Al-Ghamdi, J. Xie, Small 12 (2016) 6640–6696.
24. M. Faraldos, A. Bahamonde, Catal. Today 285 (2017) 13–28.
25. H.P. Shivaraju, Int. J. Environ. Sci. 1 (2011) 911-923.
26. T. Ohsaka, F. Izumi and Y. Fujiki, J. Raman Spectrosc., 7 (1978) 321-324.
27. A. Chatterjee, S. B. Wu, P. W. Chou, M. S. Wong, C. L. Cheng, J. Raman Spectrosc. 2011, 42, 1075–1080

28. H. Li, M. Vrinat, G. Berhault, D. Li, H. Nie, P. Afanasiev, Mater. Res. Bull. 48 (2013) 3374–3382.
29. E. Silva Junior, F. A. LaPorta, M. S. Liu, J. Andrés, J. A. Varela, E. Longo, Dalton Trans. 44 (2015) 3159–3175.
30. A. C. Ferrari, J. C. Meyer, V. Scardaci, C. Casirachi, M. Lazzeri, F. Mauri, S. Piscanec; D. Jiang, K. S. Novoselov, S. Roth, A. K. Geim, Phys. Rev. Lett. 97 (2006) 187401(1-4).
31. K. N. Kudin, B. Ozbas, H. C. Schniepp, R. K. Prud'homme, I. A. Aksay, R. Car, Nano Lett. 8 (2008) 36–41.
32. M. Spinkle, D. Siegel, Y. Hu, J. Hicks, A. Tejeda, A. Taleb-Ibrahimi, P. Le Fevre, F. Bertran, S. Vizzini, H. Enriquez, S. Chiang, P. Soukissian, C. Berger, W. A. de Heer, A. Lanzara, E. H. Conrad, Phys. Rev. Lett. 103 (2009) 226803(1-4).
33. D. Yang, A. Velamakanni, G. Bozoklu, S. Park, M. Stoller, R.D. Piner, S. Stankovich, I. Jung, D.A. Field, C.A. Ventrice Jr, S. Ruoff, Carbon 47 (2009) 145-152.
34. Y. Matsumoto, M. Koinuma, S. Ida, S. Hayami, T. Taniguchi, K. Hatekeyama, H. Tateishi, Y. Watanabe, S. Amano, J. Phys. Chem. C 115 (2011) 19280-19286.
35. L. Sun, L. Wang, C. Tian, T. Tan, Y. Xie, K. Shi, M. Li, H. Fu, RSC Adv. 2 (2012) 4498-4506.
36. C. Fu, G. Zhao, H. Zhang, S. Li, Int. J. Electrochem. Sci. 8 (2013) 6269-6280.
37. A.C. Ferrari, J. Robertson, Phys. Rev. B 61(2000) 14095-14107.
38. H. Tien, Y. Huang, S. Yang, J. Wang, C.M. Ma, Carbon 49 (2011) 1550-1560.
39. H. Shin, K. Kim, A. Benayad, S. Yoon, H. Park, I. Jung, M. Jin, H. Jeong, J. Kim, J. Choi, Y. Lee, Adv. Funct. Mater. 19 (2009) 1987–1992.
40. G. Sobon, J. Sotor, J. Jagiello, R. Kozinski, M. Zdrojek, M. Holdynski, P. Paletko, J. Boguslawski, L. Lipinska, K.M. Abramski, Opt. Express. 20 (2012) 9463-19473.
41. S. Stankovich, D.A. Dikin, R.D. Piner, K.A. Kohlhaas, A. Kleinhammes, Y. Jia, Y. Wu, S.T. Nguyen, R.S. Ruoff, Carbon 45 (2007) 1558-1565.
42. C. Xu, X. Shi, A. Ji, L. Shi, C. Zhou, Y. Cui, Plos One (2015) 1-15.
43. A. Datcu, L. Duta, A. Perez del Pino, C. Logofatu, C. Luculescu, A. Duta, D. Perniu, E. György, RSC Adv. 5 (2015) 49771-49779.
44. E. György, A. Perez del Pino, A. Datcu, L. Duta, C. Logofatu, I. Iordache, A. Duta, Ceram. Int. 42 (2016) 16191–16197.
45. G. Williams, B. Seger,P. V. Kamat, ACS Nano, 2 (2008) 1487–91.
46. E. György, A. Pérez del Pino, C. Logofatu, C. Cazan, A. Duta, J. Am. Ceram. Soc. 97 (2014) 2718–2724.
47. R. Sanjines, H. Tang, H. Berger, F. Gozzo, G. Margaritondo, F. Levy, J. Appl. Phys. 75 (1994) 2945-2951.
48. G.M. Ingo, G. Padeletti, S. Dire, F. Babonneau, Appl. Surf. Sci. 70 (1993) 230-234.

49. D. Gonbeau, C. Guimon, G. Pfister-Guillouzo, A. Levasseur, G. Meunier, R. Dormoy, Surf. Sci. 254 (1991) 81-89.
50. J.L. Ong, L.C. Lucas, G.N. Raikar, J.C. Gregory, Appl. Surf. Sci. 72 (1993) 7-13.
51. C. Párkányi, C. Boniface, J.J. Aaron, M. Maafi, Spectrochim. Acta 49 (1993)1715-1725.
52. J. N. Tiwari, K. Mahesh, N. H. Le, K. C. Kemp, R. Timilsina, R. N. Tiwari and K. S. Kim, Carbon 56 (2013) 173–182.
53. H. S. Kim, B. L. Farmer, Y. G. Yingling, Adv. Mater. Interf. 2017, 4, 1601168
54. S. Jayanthi, N. K. R. Eswar, S. A. Singh, K. Chatterjee, G. Madras, A. K. Sood, RSC Adv. 6 (2016) 1231-1242.
55. H. Wang, L. Zhang, Z. Chen, J. Hu, S. Li, Z. Wang, J. Liu, X. Wang, Chem. Soc. Rev. 43 (2014) 5234-5244.
56. H. Yan, H. Wu, K. Li, Y. Wang, X. Tao, H. Yang, A. Li, R. Cheng, ACS Appl. Mater. Interf. 7 (2015) 6690−6697.
57. P. Singh, A. Ojha, A. Borthakur, R. Singh, D. Lahiry, D. Tiwary, P. Kumar Mishra, Environ. Sci. Pollut. Res. 23 (2016) 22340-22364.
58. G. Zerjav, M. S. Archad, P. Dijinovic, I. Junkar, J. Kovac, J. Zavasnikc, A. Pintara, Nanoscale 9 (2017) 4578-4592.
59. M. Lei, N. Wang, L. Zhu, C. Xie, H. Tang, Chem. Eng. J. 241 (2014) 207–215.
60. T.F. Yeh, J. Cihlar, C.Y. Chang, C. Cheng, H. Teng, Mater. Today 16 (2013) 78-84.
61. M. Lundie, Z. Sljivancanin, S. Tomic, J. Mater. Chem. C 3 (2015) 7632—7641.
62. L. G. Guex, B. Sacchi, K. F. Peuvot, R. L. Andersson, A. M. Pourrahimi, V. Ström, S. Farris, R. T. Olsson, Nanoscale 9 (2017) 9562–9571.
63. X. Yan, T. Ohno, K. Nishijima, R. Abe, B. Ohtani, Chem. Phys. Lett. 429 (2006) 606–610.
64. Y. Liua, Y. Hua, M. Zhoua, H. Qiana, X. Hu, Appl. Catal. B: Environm. 125 (2012) 425–431.
65. K. Bramhaiah, V. N. Singh, N. S. John, Phys. Chem. Chem. Phys. 18 (2016) 1478-1486.
66. B. Ohtani, Catalysts 6 (2016) 192-197.